Long Wavelength Array (LWA): Phase Calibration Challenges and Opportunities for Ionospheric Investigations

Lightning-Ionosphere Coupling Workshop

20 - 21 August 2008

Larry P Cox [LANL]

Outline

- LWA Overview
- Basic ionospheric effects
- Phase calibration challenges
- Potential calibration sources
- Accuracy of GPS-derived TEC measurements
- Mid-latitude ionospheric structures
- An-elastic, viscous GW dispersion relation [Vadas 2008 CEDAR Prize Lecture]

Long Wavelength Array Design Concept

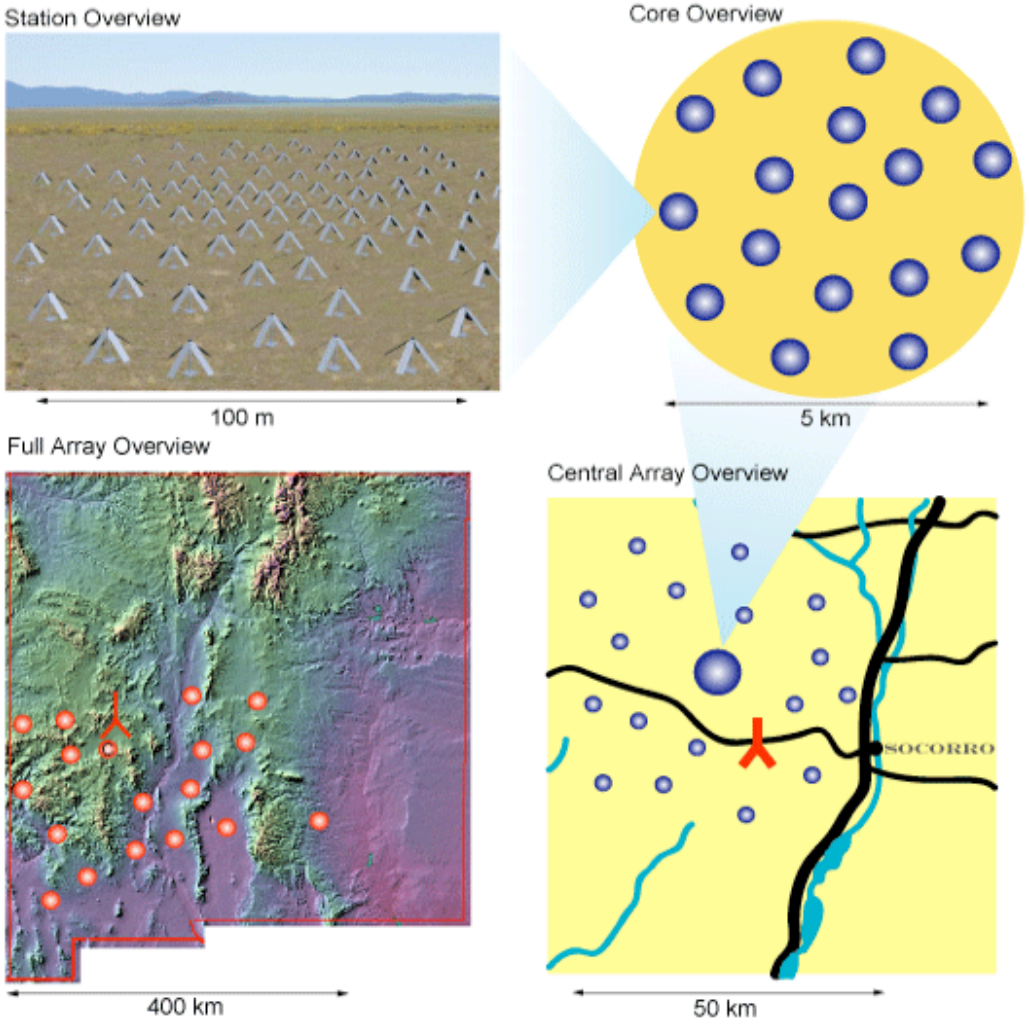

LWDA

LWDA – the Long Wavelength Demonstrator Array –The 16 dipole elements of the LWDA are seen in the foreground. In the gap between them (slightly right of center) is the *Fork* antenna (white post; the wires are not visible) and behind them to the left are the *Big Blade* antennas (with the people next to them). VLA antennas (white) are in the distance. The LWDA
algorith
in coop

Antenna Candidates

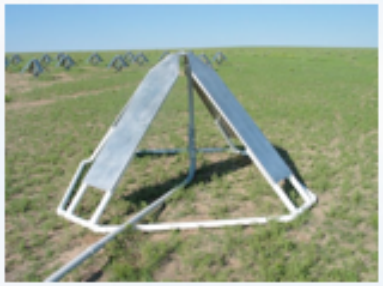

"Big Blade"

Fork

LWA Specifications

Frequency Range	10 – 88 MHz (20– 80 MHz optimized)
Effective Collecting Area	10^6 (20 MHz/ν)^{2}m^2
Number of Dipole Elements	~ 10^4
Number of Dipole Stations	~ 50
Baseline Range	0.1– 400 km
Point-Source Sensitivity (2 polarizations, 1 hour, 4 MHz BW)	1.0 mJy @ 20 MHz 0.5 mJy @ 80 MHz
Angular Resolution	15" @ 10 MHz 5" @ 30 MHz 2" @ 80 MHz
Field of View	~2° @ 80 MHz ($\propto \nu$)
Number of Independent FOV (beams)	≥ 4
Maximum Observable Bandwidth	32 MHz
Spectral Resolution	$\leq$ 1 KHz
Image Dynamic Range	$\geq 10^4$
Digitized Bandwidth	Full RF

Other low-frequency instruments in development

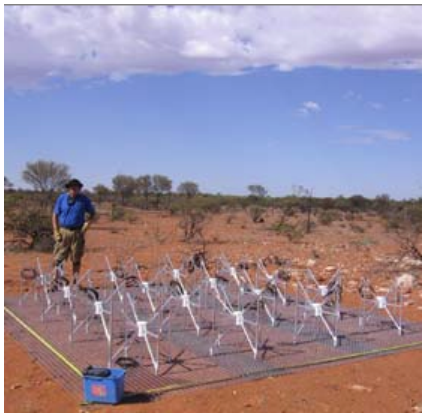

MWA 80-300 MHz

LOFAR 30 - 240 MHz

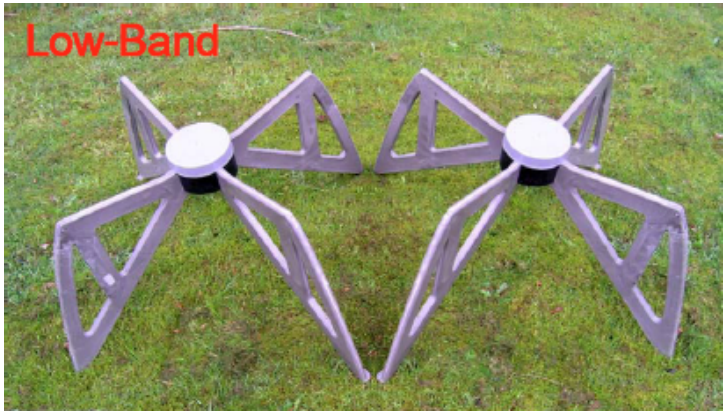

SKA 100 MHz - 25 GHz

Low-frequency radio astronomy

- A virtually unexplored field
- At low frequencies phase distortions due to the ionosphere are a significant problem in achieving high quality images
- Classical self-calibration will not work properly for large (>100km), low-frequency arrays
- Existing low-frequency arrays have larger field of view (FOV), inside which phase distortions show a gradient or even curvature

Basic ionospheric effects

- **Phase rotation by free electrons increases linearly with decreasing frequency and increasing TEC**

  $\delta\phi = 8.44 \times 10^{-7} f^{-1}$ (TEC) radians = *0.8 radians for 1 mTECU @ 10 MHz*

- **Turbulence and traveling acoustic waves cause the phase rotation to be variable in space and time; coherency timescales ~ 10's of seconds to a minute**

- **Isoplanatic patch: name given to the area of the sky over which wavefront errors are closely correlated (roughly angular measure of turbulent cell)**

  very roughly $\theta = r_0 / D$

- **Ionospheric scintillation; time coherency < seconds. Coherency lost, array not calibratable.**

Phase distortion challenges for LWA radio astronomy

- Widely separated stations 'see' entirely different regions of the ionosphere with different turbulence
- Kolmogorov turbulence and traveling acoustic waves cause the phase rotation to be variable in space and time; coherency timescales ~ 10's of seconds to a minute
- Curvature in the ionosphere for large diameter arrays causes sources to be deformed; in extreme cases a source breaks up into multiple components and coherency is lost
- Low-frequency arrays have a larger FOV for each station inside which the phase distortions have a gradient or even curvature
- Since the ionosphere changes rapidly a phase correction is needed for each integration
- Sources bright enough to be visible in one integration are needed
- A delicate balance between the timescale of rapid ionospheric phase rotations and the time to reach adequate S/N for enough calibrators to achieve a good phase screen fit
- Techniques to incorporate time coherency in phase calibration approaches is needed

Refraction: Troposphere vs Ionosphere

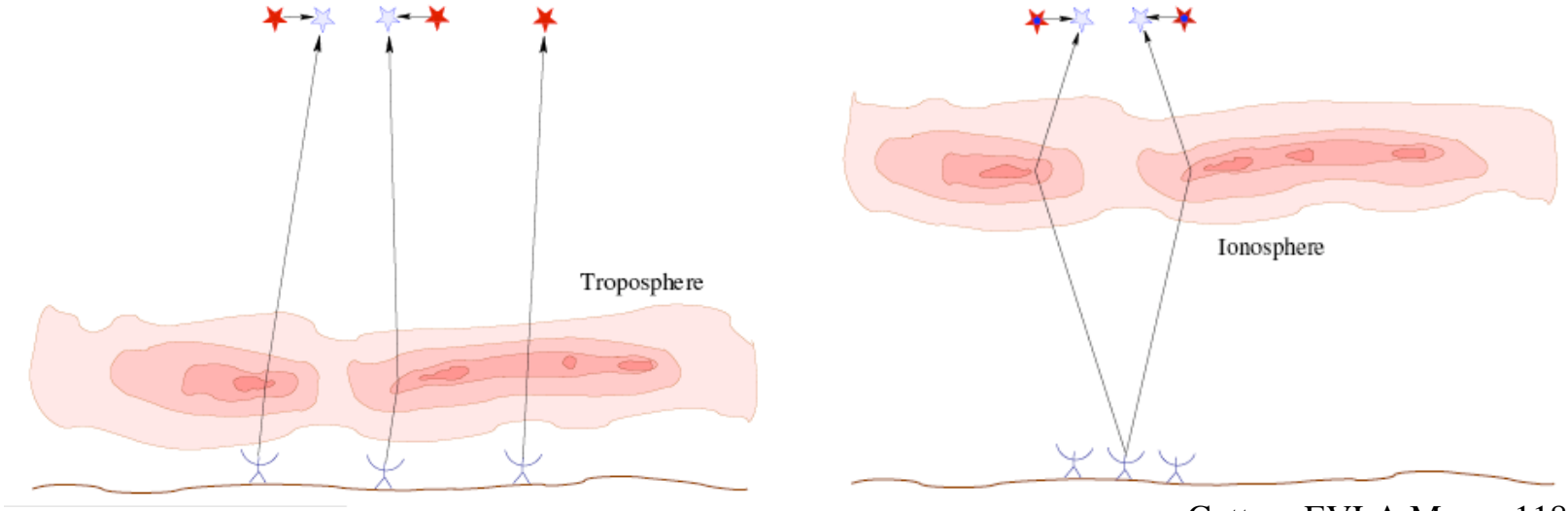

Cotton, EVLA Memo 118

shading shows relative index of refraction; lines show effects on apparent source direction

- relatively independent apparent deflections of source positions between antennas
- phase screen close to antennas
- large area of sky viewed through same portion of phase screen

- each element of array looks through nearly the same portion of the ionosphere toward a given source, but the portion of the ionosphere varies between sources
- ionospheric errors not well described by a single phase per antenna, but by a phase screen across the array

Calibration sources

The ionosphere changes rapidly (1 minute), therefore a phase correction is needed for each integration.

Therefore radio sources bright enough to be visible in one integration are needed.

The calibrators provide a collection of points projected on the ionosphere if we assume a thin layer ionosphere.

For the first iteration there is a *delicate balance* between the timescale of rapid ionospheric phase rotations and the time needed to reach adequate S/N for enough calibrators to achieve a good fit.

Field-based calibration uses low-order Zernike polynomials as the set of orthogonal basis functions to fit the phase screen.

For the VLA at 74 MHz there are seldom enough detectable calibrators to justify more than a 5 term Zernike polynomial.

Potential calibration sources

- Bright compact radio sources
  (from NVSS catalog at very different frequency and resolution)
- GPS satellites
- Satellites transmitters:
  - Orbcom constellation with 29 LEO communication satellites transmitting at 137.5 - 138 MHz

Accuracy of GPS-based TEC measurements

How accurate are absolute GPS-based TEC measurements?

How accurate are short baseline GPS-based relative TEC measurements?

What are the accuracy limitations for GPS-based TEC measurements?

Comparison of Magic (USTEC) and FORTE TEC measurements

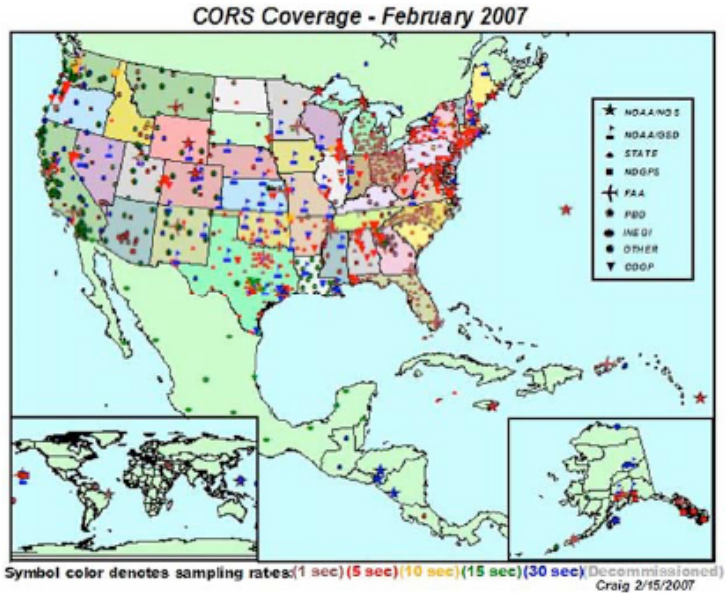

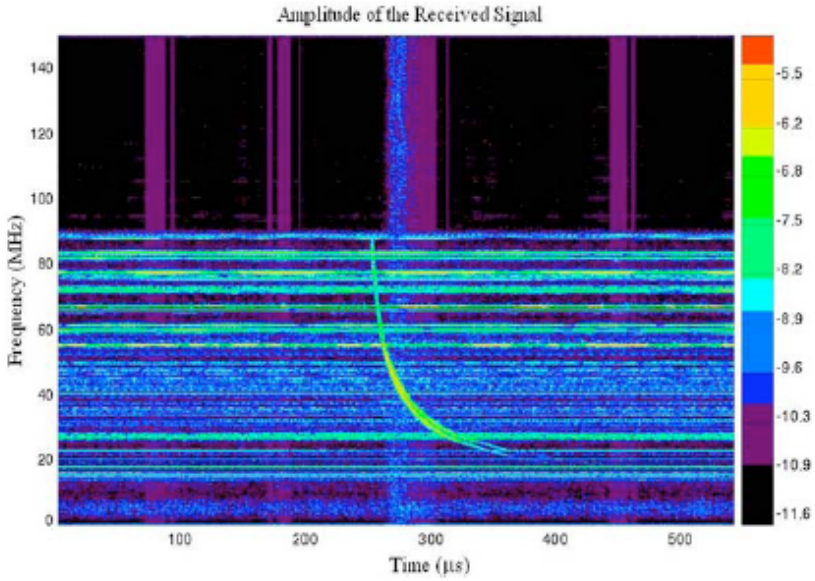

Figure 5. Moving-window spectrogram of a pulse recording by the FORTE satellite.

Minter et al, *Radio Science* (2007) U of Colorado, NOAA, LANL

Los Alamos NATIONAL LABORATORY EST.1943

NNSA

Comparison of Magic (USTEC) and FORTE TEC measurements

Table 2. Root-Mean-Square Error Calculations According to Elevation Angle Cutoff, TEC Cutoff, and Number of Stations

Average Number of CORS Stations in the Magic Solution	Average Number of CORS Stations Within 500 km of Los Alamos	Average Number of CORS Stations Within 1000 km of Los Alamos	All Data,[a] TECU	Elevation Angles > 55°,[b]	Data < 60 TECU,[c]	Elevation Angles > 55° and Data < 60 TECU,[d]
133	7	32	2.70	1.68	1.71	1.15
105	5	24	2.75	1.69	1.73	1.24
73	5	17	2.77	1.76	2.13	1.52
60	4	12	2.87	1.88	2.32	1.66
44	3	9	3.02	1.90	2.60	1.78
21	1	3	4.22	2.74	3.90	2.44

[a]Calculations used 178 FORTE observations.
[b]Calculations used 36 FORTE observations.
[c]Calculations used 84 FORTE observations.
[d]Calculations used 28 FORTE observations.

How much FORTE and Magic individually contribute to this error remains indeterminable, however the errors are expected to be unique to either system and uncorrelated.

Performance during storm conditions is unknown.

Minter et al, *Radio Science* (2007) U of Colorado, NOAA, LANL
Araujo-Pradere et al, *Radio Science* (2007) U of Colorado, NOAA

Short Baseline Relative TEC Measurements

- Two LANL NovaTel 4004B GPS receivers to be deployed starting 7/25
- Goal: To replicate short baseline relative TEC measurements reported by Skone and and Nicholson at ION GNSS 2006
- Two LANL NovaTel 4004B GPS receivers to be deployed starting 7/30 with 10 m baseline

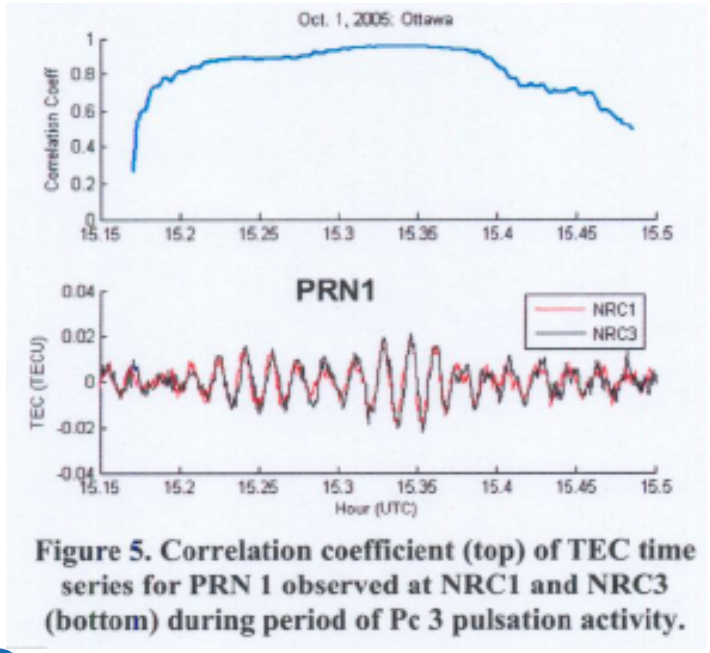

Figure 5. Correlation coefficient (top) of TEC time series for PRN 1 observed at NRC1 and NRC3 (bottom) during period of Pc 3 pulsation activity.

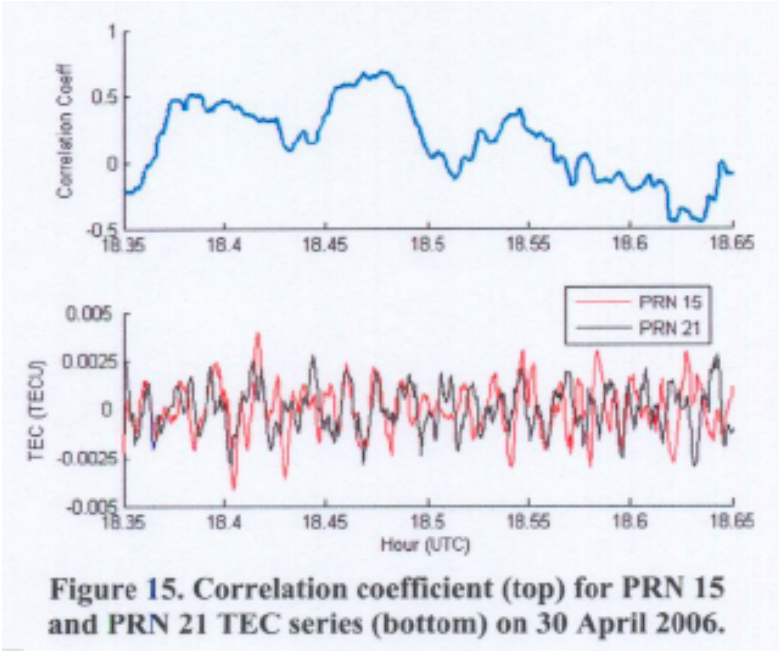

Figure 15. Correlation coefficient (top) for PRN 15 and PRN 21 TEC series (bottom) on 30 April 2006.

Skone & Nicholson (2006)

quiet solar conditions

Factors Limiting TEC Measurement Accuracy

- GPS is primarily a navigational system
  → The majority of GPS receivers are not optimized for ionospheric studies
- Introduced biases in determining TEC from a combination of absolute code derived TEC and carrier phase derived TEC:
  - Delay of pseudorange TEC as a result of code smoothing (Hatch filter)
  - Estimation rather than measurement of receiver differential code bias (DCB)
  - Ionospheric divergence of pseudorange TEC resulting from code smoothing
- More fundamentally, observed patterns of intersatellite interference between C/A codes as a function of time-varying differential Doppler shift have recently been reported [Beach and Baragona, *Radio Science*, 2007]
- In discussions with Ted Beach this summer quantitative assessments of the impact of intersatellite interference on TEC measurement accuracy await detailed GPS simulator investigation

Nongeophysical GPS amplitude fluctuations due to intersatellite interference [Beach and Baragona, 2007]

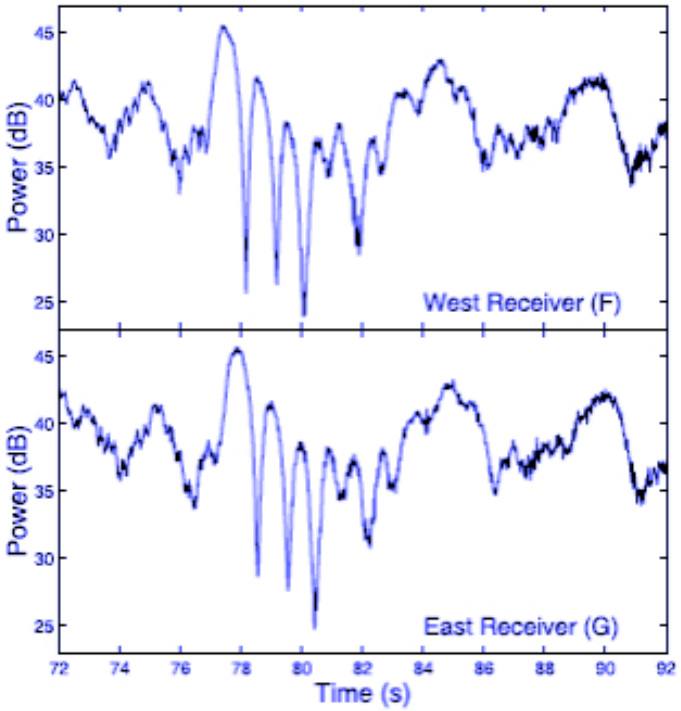

Post-correlation 50-Hz power data with significant Fresnel-type fluctuations

Cachoeira Paulista, Brazil for PRN 2 on 4 Feb 2000
55 meter baseline in geomagnetic east-west direction

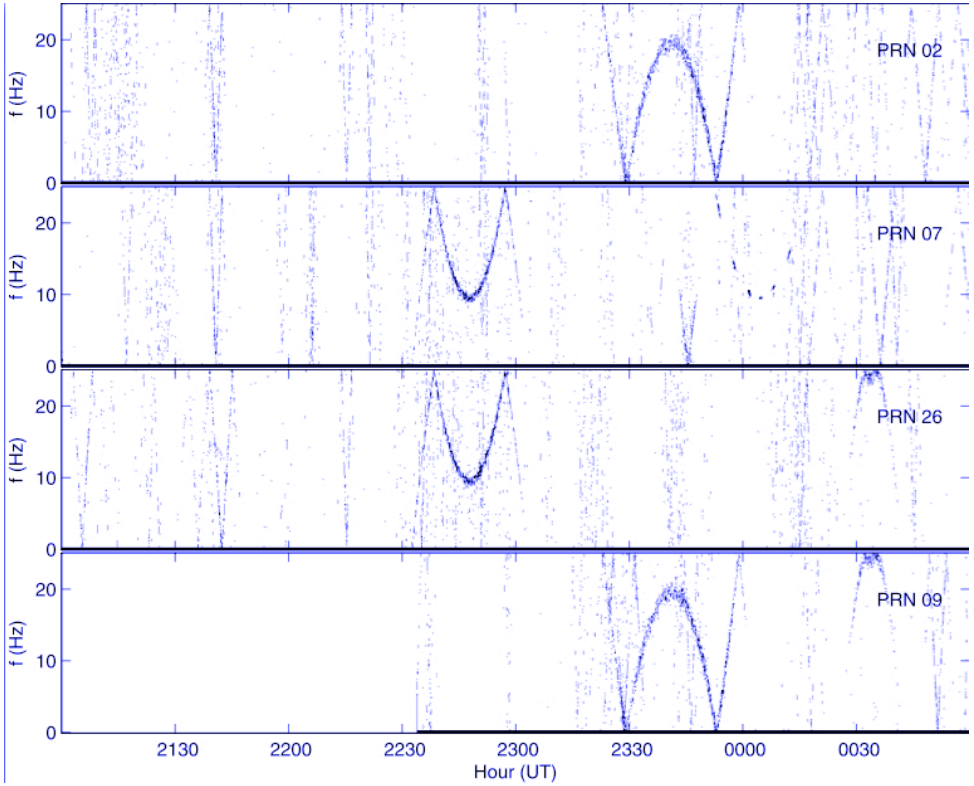

Multichannel GPS simulator tests to replicate interference patterns of 13 - 14 March 2001

Los Alamos NATIONAL LABORATORY EST.1943

NNSA

What are the dominant ionospheric structures for mid-latitude?

- TID observations in New Mexico:
  - Jacobson et al, *JGR* (1995)
    Observations of TIDs with a satellite-beacon radio interferometer
    Found bi-modal azimuth distribution of TIDs
  - Jacobson and Erickson, *Planetary and Space Science* (1992)
    Wavenumber-resolved observations of ionospheric waves using the VLA
  - Dymond et al, presented at Ionopheric Effects Symposium (2008)
    The Combined Radio Interferometry and COSMIC Experiment in Tomography (CRICKET) Campaign
- Mid-latitude turbulent upwelling:
  - Fukao and Kelley, *JGR* (1991)
    Turbulent Upwelling of the Mid-latitude Ionosphere
    1. Observational results by the MU radar

Mid-latitude ionospheric structures

The Combined Radio Interferometry and COSMIC Experiment in Tomography (CRICKET) was proposed to use VLA in conjunction with the COSMIC satellite constellation

- Following Jacobson and Erickson, we fit VLA phases assuming a plane wave model solution
  - *A. R. Jacobson and W. C. Erickson, Astron. Astrophys., 257, 401-409 (1992)*
  - *FFT the phase progression in the time domain*
  - *Fit phases for the antennas at each temporal frequency with a plane wave model*
  - *At each frequency we retrieved:*
    - Amplitude
    - Wavelength
    - Direction of travel (Azimuth)
    - Phase speed

$$\hat{\Phi}^f = \hat{\Phi}^f_m \cos(\Omega_f (t - t_0) - \vec{k}_f \circ \vec{x} + \varphi_f)$$

The "hat" denotes the FFT'd phase

- The two strong plane waves were detected
  - *Speeds and periods consistent with Acoustic Gravity Waves and MSTIDs*
- Wave 1:
  - *Period = 18.6 ± 6.3 min*
  - *Wavelength = 271 ± 16 km*
  - *Speed = 246 ± 85 m/s*
  - *Azimuth = 222° (CW N through E)*
- Wave 2:
  - *Period = 14.1 ± 3.5 min*
  - *Wavelength = 242 ± 13 km*
  - *Speed = 286 ± 73 m/s*
  - *Azimuth = 209° (CW N through E)*

ASTRA TIDDBIT HF Doppler sounder (MSTID observations)

Figure 1: Transmit Antenna (simple inverted-V, mast about 10' high,

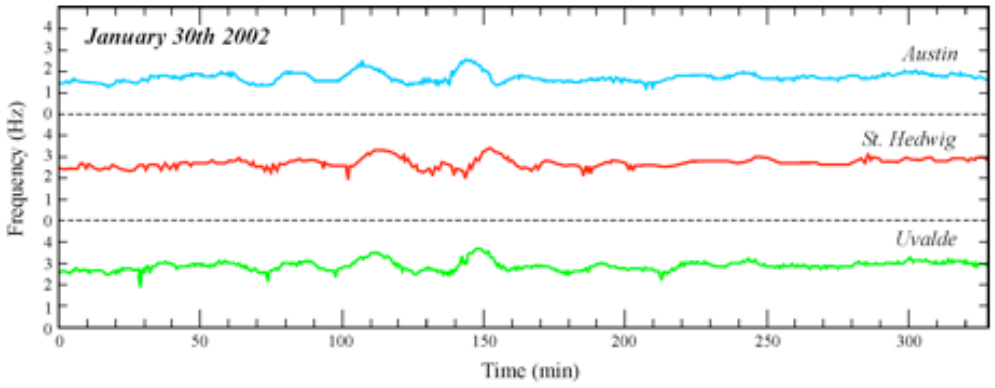

Mid-latitude turbulent upwelling structures

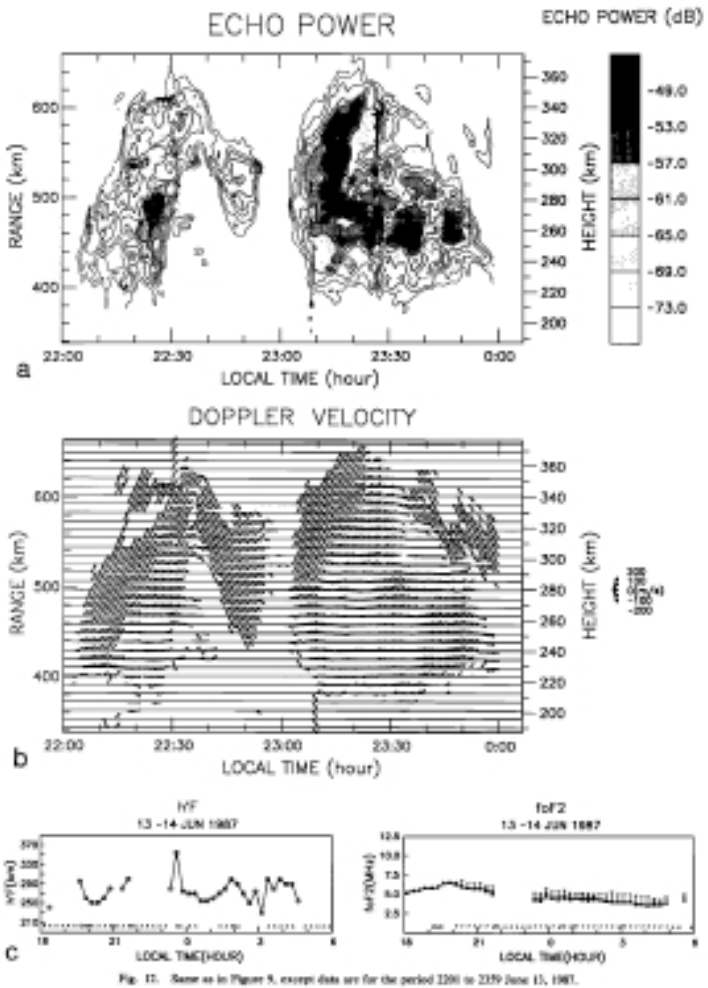

MU Radar System Parameters

Location: Shigaraki, Shiga, Japan

Geomagnetic coordinates:
- Declination = 5.7° (300 km)
- Dip angle = 48.3° (IGRF 1985)
- Dip latitude = 29.3° (IGRF 1985)

Operational freq = 46.5 MHz

Peak power = 1 MW max

Pulse length = 1-512 μs

Anelastic, viscous GW dispersion relation [Sharon Vadas 2008 CEDAR Prize Lecture]

Question posed by Dave Fritts in 2002:

Can we show via modeling that gravity waves from convection with the right scales and amplitudes are at the bottomside of the F region when plasma instabilites are seeded?

Anelastic, viscous GW dispersion relation [Sharon Vadas 2008 CEDAR Prize Lecture]

- Gravity waves carry nearly ALL momentum flux and energy (from linear response) away from typical lower-atmospheric disturbances
- For gravity waves with period less than one hour, thermospheric dissipation via kinematic viscosity and thermal diffusivity are extremely important
- Earlier analytic dispersion relations (e.g., Pitteway and Hines) break down where dissipation is strong
- Ray-tracing requires an analytic GW dispersion relation taking into account thermospheric dissipation

Anelastic, viscous GW dispersion relation [Sharon Vadas' 2008 CEDAR Prize Lecture]

$$m^2 = \frac{k_H^2 N^2}{\omega_{Ir}^2(1+\delta_+ + \delta^2/\mathrm{Pr})}\left[1+\frac{\nu^2}{4\omega_{Ir}^2}\left(\mathrm{k}^2-\frac{1}{4\mathrm{H}^2}\right)^2\frac{(1-\mathrm{Pr}^{-1})^2}{(1+\delta_+/2)^2}\right]^{-1} - k_H^2 - \frac{1}{4\mathrm{H}^2}$$

$$\mathrm{k} = (k,l,m), \quad k_H^2 = k^2+l^2, \quad \omega_{Ir} = \omega - kU - lV$$
$$\delta = \nu m/\mathrm{H}\omega_{Ir}, \quad \delta_+ = \delta(1+1/\mathrm{Pr}), \quad \nu_+ = \nu(1+1/\mathrm{Pr})$$

Includes thermospheric dissipation via kinematic viscosity and themal diffusivity

When T, U, V are constant, and P_r = 1, there is an exact solution

$$\left(\omega_{Ir} + \frac{m\nu}{\mathrm{H}}\right)^2 = \frac{k_H^2 N^2}{\mathbf{k}^2 + 1/4\mathrm{H}^2}$$

http://cedarweb.hao.ucar.edu/wiki/images/e/ed/CEDARPrizeLecture_web_Vadas.pdf

GWs propagating against the wind (West here) propagate to the highest altitudes in the themosphere

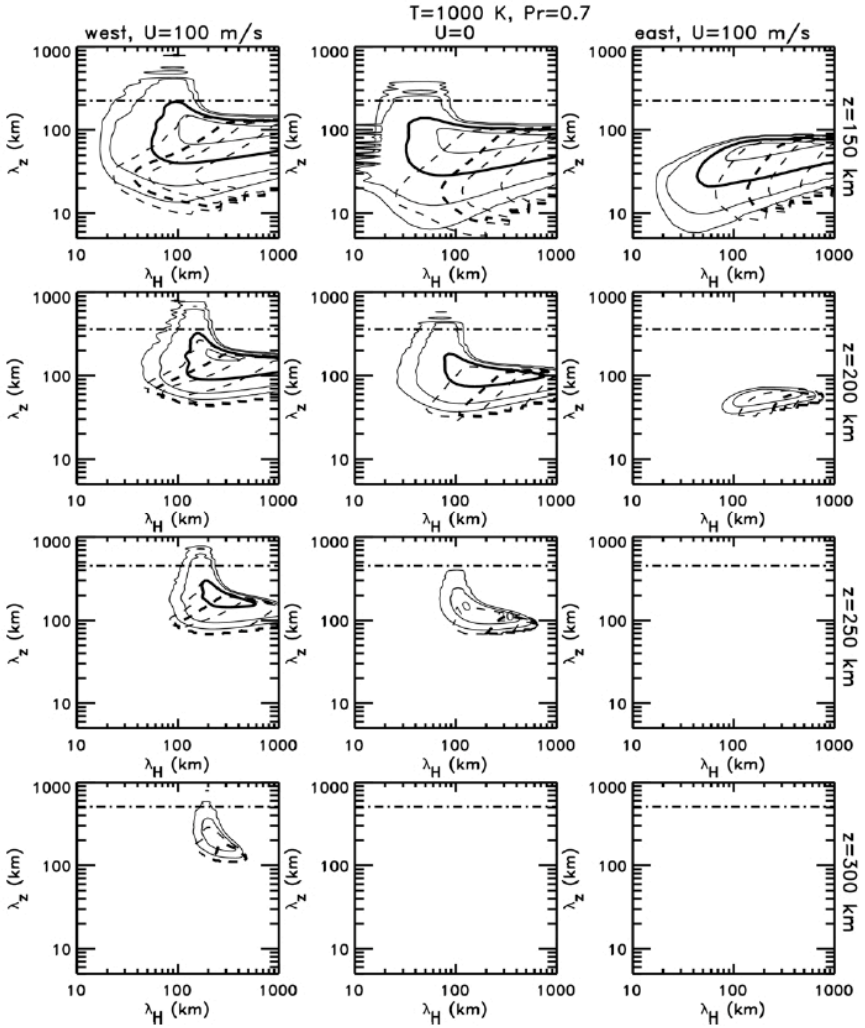

Fritts and Vadas (2008)

submitted to Annal. Geophy.

Los Alamos NATIONAL LABORATORY EST.1943

NNSA

Goal: Formulate a collaborative study plan to understand lightning- ionosphere coupling

1) Mechanisms – What are the energy coupling mechanisms?
   Neutral winds, GWs, EM waves, other
2) Observations – What observations have been made?
   What are feasible extensions?
3) Simulation resources – What codes exist?
   What is the status of validation?